Peer-reviewed and published version: 10.1109/TMBMC.2023.3265565

The Development of a Biocompatible Testbed for Molecular Communication with Magnetic Nanoparticles

Max Bartunik, Georg Fischer, Jens Kirchner

***Abstract*—Although the concept of engineered molecular communication has been around for quite some time, practical approaches with truly biocompatible setups are still scarce. However, molecular communication has a large potential in future medical applications and may be a solution to size constraints of antenna-based transmission systems. In this work, we therefore present a testbed using biocompatible magnetic nanoparticles. Based on previous work, all testbed components have been improved regarding performance and size, making a large step forward regarding miniaturisation and a data transmission approach. In addition, a setup for localised two-dimensional sensing of magnetic nanoparticles is presented. All improvements are evaluated individually and combined to achieve a net data rate of more than 6 bit/s, significantly higher than any other comparable biocompatible setup.**

***Index Terms*—molecular communication, biocompatible, magnetic nanoparticles, testbed**

I. Introduction

As miniaturisation for sensor and actor devices progresses, conventional communication concepts using electromagnetic waves become increasingly infeasible [1]. For example, envision engineered nanorobots working cooperatively on a treatment strategy in a medical context. As a generous estimate, we may assume our nanorobots to have an approximate size of 1 µm (an example for current research on xenobots in the sub-millimetre range can be found in [2]). Transmission would have to occur significantly above the terahertz band to satisfy restrictions on antenna size and would be subject to very high attenuation. Communication using electromagnetic waves would therefore be infeasible, if not even impossible.

Molecular Communication provides a possible solution for such a scenario. It is based on the idea of using molecules or other particles in the nanoscale to transmit information, similar to biological systems. Although the fundamental concept and theoretical models have been studied for some years, only few practical testbeds, which are essential to understanding relevant physical concepts and validating communication strategies, have been published. One of the first proof-of-concepts for molecular communication was shown by Farsad et al. in [3]. They presented a testbed for air-based molecular communication using alcohol as information particles with a focus on a reproducible and simple setup to facilitate further research on channel models and concepts for molecular communication. Several testbeds have been published since then (see [1], [4], [5] for comprehensive overviews of current advancements in molecular communication).

In light of medical applications for molecular communication, biocompatibility, meaning that a setup can be used in a biological system (such as the human body) without adverse effects to the system, is essential. Only very few testbeds with setups that could principally be non-toxic and could function in a biological environment have been presented. In the following, we will therefore discuss the various experimental systems for molecular communication, roughly differentiated by type of channel medium, regarding their biocompatibility. A quick overview of the most relevant testbeds is provided in Tab. I.

A. Air-based Setups

As stated above, one of the first testbeds for molecular communication uses alcohol for air-based transmission. The original concept [3] (maximally 0.33 bit/s) and derivations have been applied to validate channel models [18]–[22] or improve the transmission [16] (2 bit/s) in various other work and was extended to a MIMO setup in [23].

Other air-based setups include the use of odours [24], [25] or fluorescent droplets, released with an industrial sprayer [17]. Although the authors of [17] achieve a data rate of up to 40 bit/s, the setup relies on a dark environment and is restricted to a direct line of sight transmission (due to a ”jet”-like spray emission) making possible real-life applications very limited.

Although such air-based setups may have applications in a medical context, such as modelling the spread of an infection between patients [26], they cannot be regarded as biocompatible in the sense of in-body medical diagnostics or treatments.

B. Fluid Setups

In [6], a fundamentally biocompatible concept using pharmacokinetics to convey information as a physiological response to a controlled administration of drugs (such as through a capsule or external injection) is proposed. The authors provide a proof-of-concept in a lab environment using a setup with a peristaltic pump and table salt as information particles. They then compare their results to experimental data with drugs in both animals and humans. Data transmission is principally limited by the slow physiological body response causing a slow return to zero. Using the proposed modulation scheme with on-off keying (OOK) a data rate of less than 0.004 bit/s is achievable.

M. Bartunik, G. Fischer and J. Kirchner are at the Institute for Electronics Engineering, Friedrich-Alexander-University Erlangen-Nürnberg (FAU).

TABLE I: Selection of testbeds for molecular communication and their relevant parameters. Setups that are principally suited to function in a biomedical application scenario are marked as biocompatible. The data rate is a calculated upper boundary for the achievable data rate at a remaining bit error rate of 1 %, based on the transmission parameters.

Reference (et al. omitted)	Medium	Information Carrier	Comment	Data Rate (bit/s)	Biocompatible
Al-Helali [6]	water	table salt	pharmacokinetic model	0.004	yes
Koo [7]	saline solution	glucose	protein element to mimic skin	1.6	yes
Luo [8]	water	DNA concentration	offline setup	0.017	yes
Unterweger [9], Wicke [10]	water	SPIONs		1	yes
Farsad [11]	water	pH value	bipolar modulation	3.5	no
Grebenstein [12], [13]	balanced water	pH value	bacteria as interface	0.017	no
Khaloopour [14]	water	pH value	monopolar modulation	0.04	no
Wang [15]	water	table salt		7.8	no
Farsad [3]	air	alcohol		0.33	no
Lu [16]	air	alcohol	development from [3]	2	no
Damrath [17]	air	fluorescence	jet spray emission	40	no

The authors of [7] utilise a syringe pump and glucose receiver to modulate data as a change of glucose concentration carried in a channel with active background flow, simulating a blood stream. Again, OOK is used as modulation technique with an achievable data rate that is restricted to maximally 2 bit/s. However, due to transmission errors the actual data rate is lower. This testbed was specifically developed with biomedical applications in mind. A principal biocompatibility is demonstrated using a protein layer to simulate skin and by constructing an implantable receiver.

Another molecular communication system is based on the modulation of pH value in a fluid environment. A tabletop demonstration using peristaltic pumps to inject an acid or base in an active background flow of water is shown in [11]. The authors employ various demodulation techniques, including deep learning, to achieve a data rate of up to 4 bit/s. A possible addition to this concept is shown in [12], [13], where Escherichia coli bacteria are used as a biological interface to modulate pH value based on external optical stimuli (the feasibility of a similar receiver design was shown in [27]). Due to the kinetics of the bacteria's ion pumps, the data rate is limited to 0.017 bit/s, in contrast to the tabletop setup [11]. In [14], the same concept is applied with a wider communication channel, but only using monopolar pH modulation with an acid, achieving a data rate below 0.04 bit/s. However, pH modulation is very limited in respect to biocompatibility. Often the tolerable pH variation in a biological environment is very restricted and strongly effected by noise caused by other pH actors (such as acid-base homeostasis).

The authors of [15] achieve a bit error rate of 5 % for a transmission with 10 bit/s by modulated injections of saline solution in a water channel, detected as changes in conductivity at the receiver. The high data rate is primarily achieved by using a demodulation scheme with detailed channel memory. Similarly to pH modulation, data modulated through salinity would be subject to severe background noise in typical biological environments and can therefore not be regarded as biocompatible.

In [8], a testbed using DNA as information carrier is presented. Unlike in nature, information is however not encoded within a DNA strand but, using concentration shift keying (CSK), by selectively releasing an amount of DNA strands from a surface, controlled by an external electric signal. The DNA concentration is then measured at the receiver using a commercial offline sampling device. The authors claim a potential data rate of 0.017 bit/s. Although this method is promising for biomedical applications, the demonstrator is not sufficiently developed for a continuous transmission. Most importantly, each symbol requires manual sampling as no method for in-system symbol detection has been developed yet.

All these setups reproduce biological signalling or use naturally occurring information molecules. A different approach for a biocompatible setup was presented by some of the authors in [9]. The authors propose the use of synthetic magnetic nanoparticles (MNP) to transmit data in an active background flow. An original data rate of 0.16 bit/s is achieved using the proposed testbed, consisting of a peristaltic pump as transmitter and a susceptometer as receiver. These results are improved upon in [10] to reach 1 bit/s. The MNPs are biocompatible, making medical applications possible.

Microfluidic setups with lab-on-chip approaches have also been proposed as testbeds for molecular communication (e. g. using coloured droplets [28], [29] or polystyrene beads [30]). However, as the focus is on lab systems, they are typically not biocompatible.

C. Primary Contributions

In this work, we will show various major improvements regarding robustness, scalability and the achievable data rate to the concept presented in [9]. These include the implementation of a micropump as transmitter, improvement and evaluation of the physical transmission channel, three new receiver concepts and the application of deep learning for demodulation. The improved testbed components are an order of magnitude smaller than the initial implementation, a significant step towards miniaturisation.

Regarding the transmission channel, the contribution presented in [15] is the closest to the work shown here. However, in contrast to the setup using salt, we use MNPs with specifically detectable magnetic properties independent of the biological environment. The highest achieved data rate in a comparably biocompatible setup [7] is 1.6 bit/s. Using CSK in the new testbed we reach a significantly higher data rate of more than 6 bit/s.

Furthermore, for the first time in molecular communication, we present a setup allowing for two-dimensional localised detection of MNPs using planar coils. The sensor setup is evaluated in the overall testbed setup.

Finally, we also provide an in depth comparison of the improved testbed components as a potential aid for similar testbed setups.

II. Concept

The developed testbed focusses on water-based transmission of data using concentrations of information particles to encode information. The transmitter injects an amount of particles into the transmission channel, which are carried by an active background flow to a receiver. The transmission quality depends on many factors, such as the used particle concentration and volume, the transmission channel parameters and the receivers' sensitivity. In this work, we will present the various improvements and developments made both on the receiver and transmitter sides since the original concept was presented in [9]. The aim is to maximise the effective data rate, assuming a fixed transmission channel.

The components of the testbed can be grouped in the categories information carriers, transmitters, channel and receivers. In the following sections we will outline the relevant aspects of the individual components and show the improvements made in each category.

An overview of major component iterations made for transmitters, receivers, and the geometry of particle injection into the transmission channel is shown in Fig. 1.

III. Information Carriers

We use magnetic nanoparticles (MNPs), specifically superparamagnetic iron-oxide nanoparticles (SPIONs), as information carriers in our testbed. The SPIONs are synthesised by the Section for Experimental Oncology and Nanomedicine (SEON) of the University Hospital in Erlangen using co-precipitation [31]. The miniature beads that make up the SPIONs core consist of ferromagnetic material. Due to their small size, only one magnetic domain is formed in each bead, hence they show no remanence (essential for avoiding particle agglomeration in medical applications) and therefore behave like paramagnetic material. However, as they show a high susceptibility they are referred to as superparamagnetic.

The iron core is covered with a protective, biocompatible coating of lauric acid to avoid agglomeration. The whole particle has a hydrodynamic diameter of approximately 50 nm. It is possible to also produce magnetic nanoparticles with different sizes and coatings. Furthermore, the coating can be functionalised, for instance for drug delivery. An extensive overview regarding SPIONs in biomedical applications can be found in [32].

The high susceptibility χ can be used to detect the SPIONs using the magnetic field produced by a coil. Similarly, a capacitor can be used to sense SPIONs as a shift in relative permittivity

$$\kappa = \chi + 1. \tag{1}$$

As the authors were able to show in [33], [34], the magnetic properties of the SPIONs can also be used to direct and locally concentrate the particles with the aim of targeted drug delivery.

IV. Transmitters

Information carriers are emitted into the transmission channel using one or multiple pumps. These are computer controlled to accomplish OOK or CSK. The geometry of the transmitter injection into the transmission channel will be discussed separately in Section VI.

Transmitters, in the context of this testbed, are devices that inject information particles into the transmission channel stream. Transmitters ideally are able to perform an infinite amount of injections without variations. To maximise the signal amplitude at the receiver, a high dispensing speed (flow rate) is desirable. If an injection burst is dispensed slowly and therefore distributed in the transmission channel, the localised concentration achieved at the receiver is lower. Furthermore, the maximally possible data rate at the transmitter is limited by the time needed to inject a symbol and the information encoded in a symbol.

For our testbed, we first investigated the use of peristaltic pumps and later advanced to micropumps as transmitters. Important transmitter parameters are timing precision, injection volume precision and flow rate. In the following, we will outline the two different pump systems used as transmitters in the testbed.

A. Peristaltic Pump

Initially, a commercial peristaltic pump (Ismatec REGLO Digital ISM596D) with twelve rollers was used [9], [35], [36]. The choice of tubing defines both the maximal flow rate and the minimal dispensing volume. As a trade-off, a tube with an inner diameter of 1.52 mm (Ismatec Tygon ST), resulting in a maximal flow rate of 17 mL/min, was used. The pump can be controlled via a serial interface. A graphical user interface (GUI) to enable injections based on binary input was developed accordingly.

The peristaltic pump presented an initial proof-of-concept but was not an optimal solution. Due to its size of 10.2 cm by 13.5 cm by 17.8 cm it is unsuitable for compact setups. Furthermore, the volume flow is ramped up/down at the beginning/end of an injection by the firmware of the pump, extending the injection period.

B. Micropump

After demonstrating the feasibility of the transmitter setup [9], [35], micropumps were employed as a compact transmitter alternative [37]. We used piezoelectric micropumps, manufactured by Fraunhofer EMFT in Munich. The pump chamber membrane is attached to a piezoelectric actuator that is bent when a voltage is applied to it. The volume dispensed per pump stroke therefore depends on the applied voltage and is approximately 10.5 µL for a full pump stroke. Injections with a larger volume can be achieved by performing multiple pump

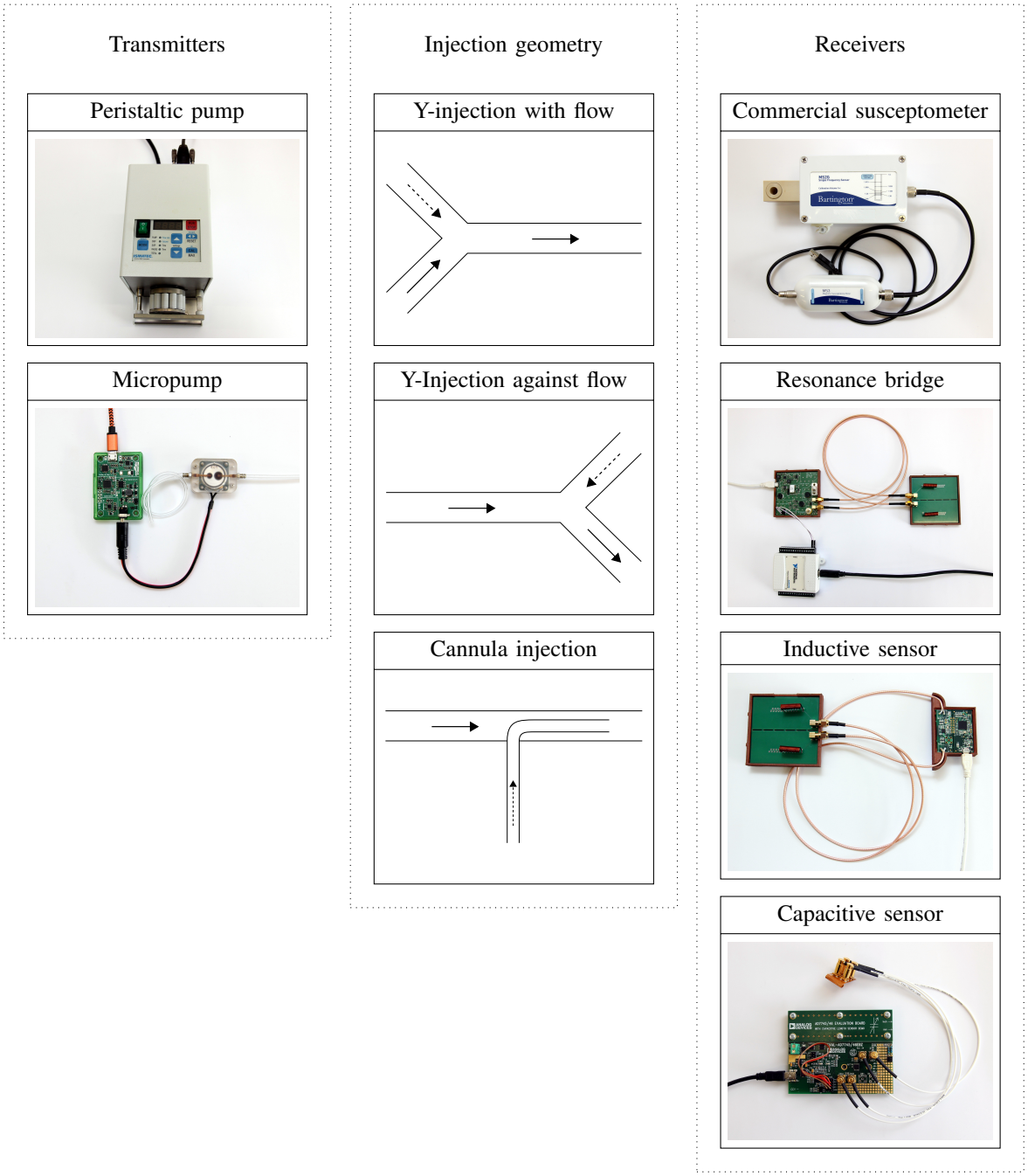

Fig. 1: Overview of the components used as transmitters, receivers, and to inject information particles into the transmission channel in the various testbed iterations. Details about each component and comparative evaluations can be found in Sections IV through VII.

strokes with a high frequency (typically 40 Hz). The pump has a diameter of 20 mm and a height of 1 mm. To enable continuous transmission, custom firm- and software was developed, that transfers data to a ring puffer implemented on the pump controller. By using a variety of injection volumes, the transmission could be extended from binary OOK to more complex symbols with CSK. In comparison to the peristaltic pump, the size of the transmitter is reduced by one order of magnitude, from the cm to the mm scale.

C. Comparison of Pump Flow

The flow behaviour of the different transmitter systems was evaluated using the SLF3S-1300F flow sensor from Sensirion. Each pump was directly connected to the sensor and operated with water and a constant flow rate of 10 mL/min.

Fig. 2 shows the resulting flow behaviours, taken from a continuous measurement with 200 samples per second. The flow speed oscillation for the peristaltic pump has a dominant frequency of approx. 20 Hz, corresponding to the individual pump rollers rotation. Additional harmonic frequencies are

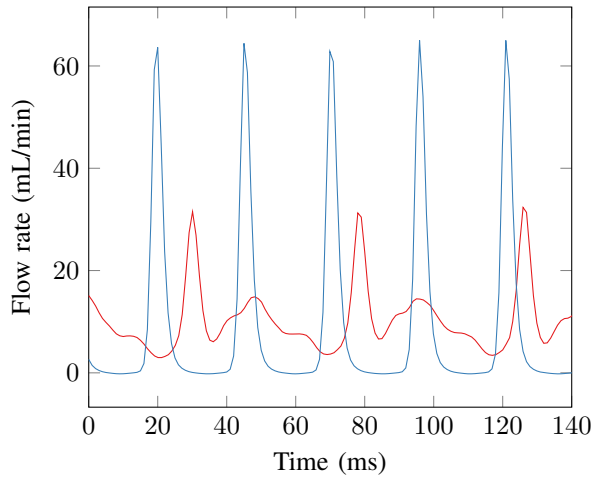

Fig. 2: Comparison of time dependent flow rate for the peristaltic pump (red) and the micropump (blue). In both cases the average flow rate is 10 mL/min.

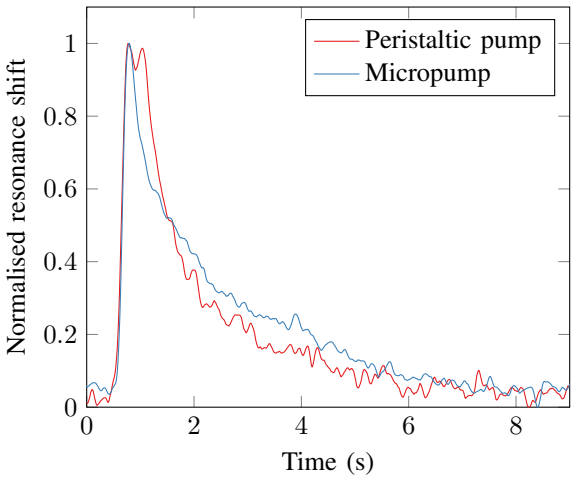

Fig. 3: Comparison of the impulse response measured at the receiver for an injection using either the peristaltic pump or micropump. Twenty individual injection bursts were recorded and averaged for each pump. The recorded peak for the peristaltic pump is broader due to the lower peak flow rate.

caused as multiple rollers come in contact during a transition period. For the micropump we see a clear dominant frequency at the pump's operation frequency of 40 Hz. Each peak corresponds to one pump stroke with a high flow rate, that returns to zero in between strokes. Higher deviations in the time dependant flow rate are mitigated by the doubled operation frequency.

D. Comparison of Pulse Injection

For a data transmission scenario, the impulse response, measured at the receiver, is especially significant. We therefore used the pump systems to inject a single burst of SPIONs into the transmission channel and recorded the received signal. This was repeated twenty times. The resulting impulse responses were overlapped by finding the maximal cross-correlation and averaged, ignoring the two strongest outliers. Fig. 3 shows the averaged pulses.

The impulse response for the peristaltic pump has a broader peak than the micropump. This is due to the lower peak flow rate, causing a longer injection period for the peristaltic pump. Furthermore, the falling slope for the micropump is smoother as, unlike with the peristaltic pump, some residual forward flow occurs after the end of an injection.

E. Reducing Backflow

Depending on the injection geometry (see Section V), information particles may be pushed back from the point of injection by water from the background flow. Especially during long time periods with no injections this can cause a reduced injection volume for the first burst after such a period. To mitigate this effect, we employ a one-way check valve from Elveflow to stop backflow directly at the needle connection. The valve is normally closed and opens with a forward pressure greater than 1200 Pa.

Fig. 4 shows a sample receive pulse after an injection pause of 60 s, with and without the additional valve. Without the check valve no peak can be detected, while the injection burst is clearly visible when using the valve.

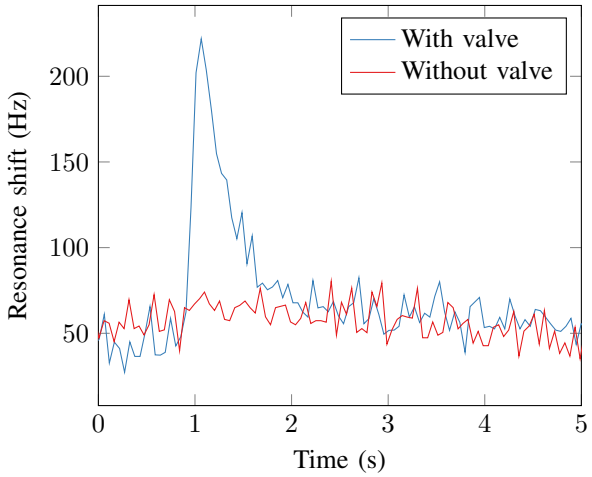

Fig. 4: Recorded receiver signal for an injection burst of SPIONs with and without a backflow stop valve. The burst was sent after a 60 s period with no injections. As SPIONs are pushed back from the injection point during periods with no transmission, no burst can be observed when the valve is not used.

F. Discussion

Both pumps can be used for a transmission scenario, however the higher peak flow rate of the micropump makes it more suitable for short symbol intervals. Furthermore, the micropump is an order of magnitude smaller than the peristaltic pump and one step closer to miniaturised applications.

The use of a one-way check valve avoids backflow during periods with no injections and therefore results in a more constant dispensing behaviour.

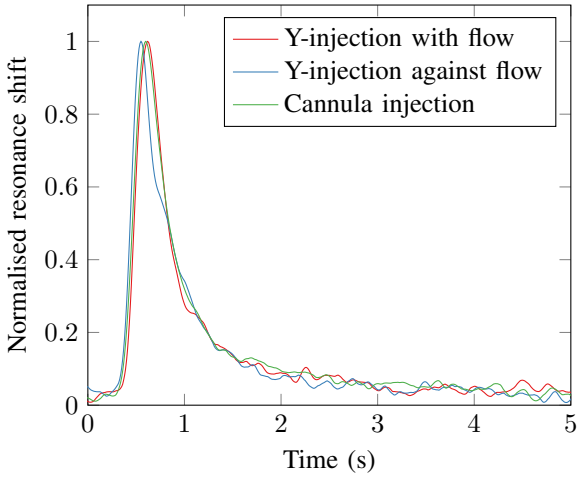

Fig. 5: Comparison between the impulse responses recorded for three different injection geometries. No significant difference can be observed, allowing for comparable measurements with different injection geometries.

V. Injection Geometry

The mechanical connection at the point of injection can influence the particle behaviour inside the transmission channel. Depending on the injection and channel geometry, an injection burst may be distributed evenly in the cross section of the channel or be focused in the centre or at any other point. We will however restrict ourselves to an injection using a Y-connector or a venous cannula. In a real-life application this would typically be a fixed requirement of the system (such as a blood vessel).

In the original setup [9] a Y-connector placed with the direction of flow, as shown in Fig. 1, was used. However, this caused particles to constantly be washed out of the injection channel into the transmission channel. By placing the Y-connector with the injection direction against the background flow, this effect could be mitigated. In a medical application a Y-connector is however not typically given. We therefore employed venous cannulas with an inner diameter of 0.7 mm to achieve a needle injection along the transmission channel.

Fig. 5 shows the impulse response recorded at a receiver using the different injection geometries. As before, 20 injections were performed for each geometry to then calculate an average signal. The impulse response is similar for all three injection geometries. This is due to the dominant effect of turbulence at the point of injection, causing a similar particle distribution. Therefore, a direct comparison between measurements taken with different injection geometries is possible.

VI. Channel

The transmission channel consists of tubing, that can be chosen or modified to represent a specific real-life application. To evaluate the testbed improvements, we consistently used a tube with an inner diameter of $D = 1.52\,\mathrm{mm}$ and a typical distance of 5 cm from the point of injection to the start of the receiver.

A background flow, with a flow rate of $Q = 10\,\mathrm{mL/min}$, is upheld using a peristaltic pump (Ismatec Reglo ICC). The Reynolds number, defined as

$$\mathrm{Re} = \frac{\rho V D}{\mu} \tag{2}$$

with the fluid density ρ, flow velocity

$$V = \frac{Q}{\pi D^2} = 0.023\,\mathrm{m/s} \tag{3}$$

and dynamic viscosity μ, provides an estimation for the applicable flow regime. Assuming the dynamic viscosity and density for water at standard temperature and pressure, our testbed conforms to $Re << 2300$. We can therefore safely assume laminar flow inside the transmission channel [38].

A. Length Variation

The influence of length variation on a transmitted particle burst were investigated using the inductive sensor described in Section VII-B to record the distribution of the particle concentration at different distances from the injection point. Ten injections were performed for each distance and the characteristic values of maximal amplitude and full width at half maximum (FWHM) calculated for each injection pulse. Fig. 6 shows the average values and corresponding standard deviation observed for a length of 0 cm to 40 cm. As the channel length increases, the amplitude caused by the injection burst decreases. This is due to the laminar flow profile, causing an axial distribution of the injected burst as it travels through the transmission channel. Therefore, the peak concentration and burst length at the receiver depend on the channel length. Similarly, the FWHM and, as noise becomes more dominant, its deviation increases with the channel length.

In a data transmission scenario, the transmission parameters must be optimised for a given channel length and flow rate. Possible approaches to mitigating the negative impact of an increased channel length are increasing the injection volume or the symbol interval.

For all other experiments a fixed channel length of 5 cm was chosen to compare the different testbed components. At this distance, the amplitude of an injected particle burst is attenuated by 3.6 dB in comparison to a measurement at the point of injection.

VII. Receivers

As SPIONs have a high susceptibility, they can be detected based on their interaction with a magnetic field (f. e. as produced by a coil). This principle is used in susceptometers. Initially, a commercial susceptometer (MS2G and MS3 sensor system from Bartington) was used [9]. However, the commercial device has a fixed aperture, causing a loss of sensitivity for smaller transmission channels. Furthermore, the sample rate is restricted to 10 samples per second, which is insufficient for data transmission scenarios with reduced injection intervals [35].

We therefore constructed several generations of custom sensing devices, which were optimised regarding adaptability to the testbed, sensitivity, and sample rate.

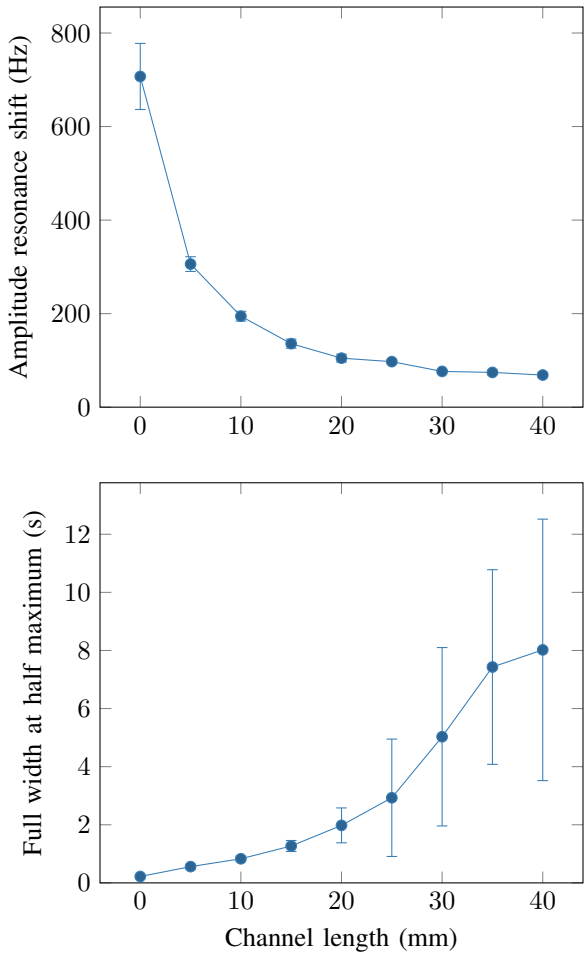

Fig. 6: Amplitude resonance shift and FWHM measured for an injection burst with a channel length of 0 cm to 40 cm. The burst is distributed more as the channel length increases, causing a reduction in peak amplitude and an increase in pulse width.

A. Resonance Bridge

Building on the same principle as the commercial susceptometer, we constructed a sensor device with a measurement coil. The custom-made coil is operated as a parallel circuit with a capacitor in a resonance bridge with a second reference coil [35]. A shift in the coil inductance

$$\Delta L = \Delta\mu_\mathrm{r}\frac{\mu_0 N^2 A}{l} = \Delta\chi\frac{\mu_0 N^2 A}{l} \tag{4}$$

with N windings, cross sectional area A, and length l, as it is caused by a change of core susceptibility $\Delta\chi$, effects a shift in the resonance frequency of the parallel circuit and results in a non-zero ac signal across the resonance bridge. An envelope demodulator and a data acquisition card are used to digitally record the susceptibility value. The reference coil reduces measurement errors caused by changing environment conditions, such as temperature or a magnetic field. The whole resonance bridge is operated at a fixed frequency of 10 MHz.

The sensor requires a difficult manual tuning procedure to adjust the resonance circuits to the fixed operating frequency, which has a large impact on sensitivity. We therefore developed other receivers, presented in the following sections.

B. Inductive Sensor

Similar to the resonance bridge, the inductive sensor relies on a shift of resonance frequency to detect SPIONs [36]. However, using the commercial inductive sensor LDC1612 from Texas Instruments, a parallel circuit of measurement coil and capacitor is driven at resonance frequency and the shift in resonance measured, instead of a resulting bridge imbalance. In this way, a manual tuning procedure is not necessary.

In initial experiments, a high dependency on environment temperature and a temperature drift was observed during operation. We therefore used capacitors with a high rating for temperature stability and, as before for the resonance bridge, used a second coil as base reference.

C. Capacitive Sensor

An alternative detection method is the use of a capacitor to measure a shift of permittivity

$$\Delta\varepsilon = \Delta\varepsilon_\mathrm{r}\varepsilon_0 = \Delta\chi\varepsilon_0 \tag{5}$$

caused by a change of susceptibility $\Delta\chi$ in the transmission channel. Assuming two parallel capacitor plates with a surface A and a distance d, the resulting shift in capacitance is

$$\Delta C = \Delta\varepsilon\frac{A}{d} = \Delta\chi\varepsilon_0. \tag{6}$$

We therefore constructed a receiver using the capacitance-to-digital converter AD7746 from analog devices [39] and two flexible capacitor planes, with a surface of 43 mm^2. The flexible printed circuit board (PCB) was wrapped around the transmission channel, resulting in a capacitor with nearly parallel plates. The outside layer of the PCB is covered with a ground mesh to reduce interference.

The capacitor is driven with a 32 kHz excitation source, causing a changing electric field and a non-zero magnetic field $\vec{B}$ between the capacitor planes, that deteriorates at the edges. According to [40] the force experienced by an object of volume V with susceptibility χ_obj in a medium with susceptibility χ_med can be described as

$$\vec{F} = \frac{1}{\mu_0}\left(\chi_\mathrm{obj} - \chi_\mathrm{med}\right) V \left(\vec{B}\cdot\vec{\nabla}\right)\vec{B}, \tag{7}$$

demonstrating that a particle with a higher susceptibility than the surrounding medium will experience a force towards the higher magnetic field strength. In our setup, this causes a broadened impulse response at the receiver, as SPIONs are attracted towards the magnetic field inside the capacitor and take a longer time to be washed out [39]. This effect could be reduced by using a lower excitation frequency, causing an increased sample time, smaller capacitor planes or a lower excitation voltage, which would both impact the sensitivity.

TABLE II: Comparison between the used sensor devices regarding sensitivity. The capacitive sensor with the constructed flexible capacitor exceeds the SNR of all other devices.

Sensor	SNR (dB)
Commercial susceptometer	138.07
Resonance bridge	66.97
Inductive sensor	128.65
Capacitive sensor	170.38

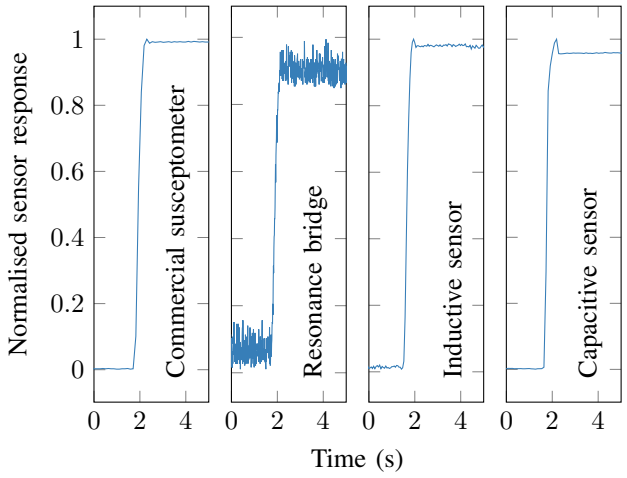

Fig. 7: Sensitivity samples for the four investigated sensors. Initially, the sensors are filled with water. Then they are quickly flushed with SPIONs. The comparatively low SNR of the resonance bridge is clearly visible. The other three devices have similar results, whereas the relative noise level of the capacitive sensor is lowest.

D. Sensitivity Comparison

One of the most important characteristic for a sensor device is sensitivity. We therefore measured the signal-to-noise ratio (SNR) for each receiver to compare the different sensors' performance. To this end, the transmission channel was filled with SPIONs at a concentration of 7.5 mg/mL and then completely flushed with water. A sample of 1.5 s was taken for both the signal and the noise value. Noise power was calculated as the root mean square, the signal amplitude as the mean of the signal sample.

Samples of the measured sensor responses are shown in Fig. 7, the calculated results for the four sensors in Tab. II. The resonance bridge has the lowest SNR value, with a significant distance to the other sensors' sensitivities. Both the inductive sensor and the commercial susceptometer have similar results with a distance of 10 dB between them. The capacitive sensor significantly exceeds the SNR of all other devices.

E. Two-Dimensional Localisation

In addition to one-dimensional nanoparticle concentration sensing, a more localised detection of MNPs would enable a better understanding of particle flow and allow for spatially modulated encoding. In our testbed this can be achieved by replacing the custom-made wire-wound coils with planar coils, that can be placed at different angles on the outside of the transmission channel. We used two commercially available planar coils (LDCCOILEVM from Texas Instruments) with 35 turns, 2 layers and a diameter of 29 mm. The coils were placed on each side of the transmission channel.

We evaluated the localisation accuracy with a peristaltic pump (Ismatec Reglo ICC) and two injection cannulas, one on each side of the transmission channel, separated into two sections by inserting a plastic foil strip. A constant injection flow with an individually varying flow rate was applied to the injection channels. While the flow rate for the first channel was decreased from 9 mL/min to 1 mL/min the flow rate for the second channel was increased from 1 mL/min to 9 mL/min within 20 s.

Fig. 8 shows the resulting average difference in resonance shift between both planar sensor coils and the appropriate standard deviation for ten individual measurements. A linear relation between the resonance shift difference and the particle concentration difference is clearly visible, proving the viability of two-dimensional spatial detection of MNPs in the transmission channel. The non-zero centre value is due to slight variations in sensor placement, injection geometry, pump behaviour and an imperfect channel separation.

The localised detection of particles demonstrated here may be particularly interesting when investigating particle distributions and movement (e. g. influence of localised turbulence, dynamics of two joining flows). However, localisation-based modulation is difficult to achieve reliably, as it is impacted by channel noise (e. g. turbulence at the point of injection) and crosstalk.

VIII. Data Transmission

The components described above are combined in the testbed shown in Fig. 9 to transmit data, modulated as a change of SPION concentration over time (CSK). Different amplitude levels for CSK are achieved by varying the intensity and amount of pump strokes made per injection. Each amplitude level increases by an injection volume of approx. 5 µL, corresponding to half a pump stroke. Due to the high injection frequency of 40 Hz, multiple pump strokes are observed at the receiver as a single injection with higher volume.

The signal recorded at the receiver is demodulated using a Convolutional Neural Network (CNN) implemented in Python [39]. To this end, the transmission is split into individual symbols using the known symbol interval. The symbols are then passed to the trained CNN for prediction of the transmitted symbol.

The use of less computationally expensive demodulation methods, such as Linear Discriminant Analysis (LDA) [37], [41] with three features per CSK symbol (rising edge height, falling edge height and maximal amplitude), has also been investigated. However, better results were achieved using the CNN predictor. Nonetheless, LDA is a viable alternative for setups with restricted computational capabilities at the receiver.

To evaluate the complete data transmission setup, a random sequence of 2000 symbols with eight different amplitude values and a symbol interval of 0.3 s (10 bit/s gross data rate),

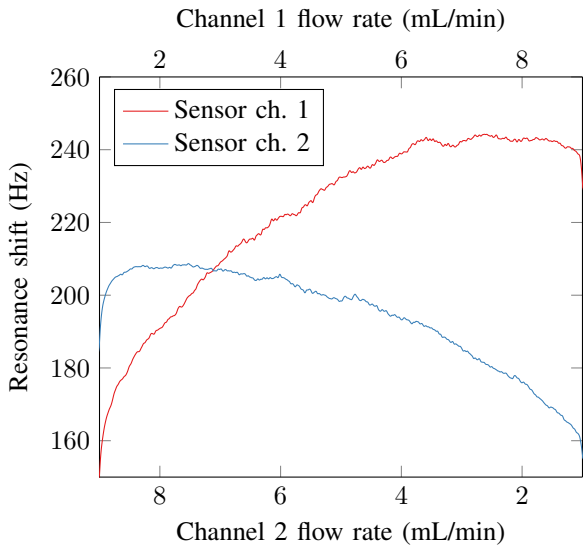

(a) Average responses to the change in relative particle concentration for each of the two inductive sensors. The different resonance shift magnitudes are due to tolerances in pump behaviour and sensor placement.

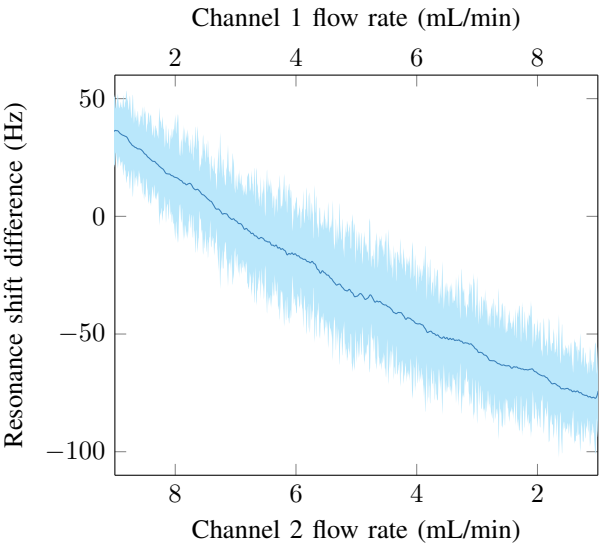

(b) Average resonance shift difference and standard deviation for ten measurements. The linear relation to the effective concentration shift in the transmission channel shows that two-dimensional localisation is possible.

Fig. 8: Localisation performance evaluation using two planar coils. Constant injection flows with individually varying flow rates were used to inject MNPs in a split transmission channel.

was recorded. To simplify automated transmission detection the symbol sequence was prepended and appended by a standardised sequence of seven symbols (7000007). The recorded symbols were then split into a training set (80 %), a validation set (10 %), and a test set (10 %).

A bit error rate of 8.43 % (i. e. noise level) was achieved using the described decoder and grey code for symbol representation. According to Shannon's theorem the achievable code rate R for a given binary channel with noise level f and a tolerable remaining bit error probability p_b is

$$R = \frac{1 - H_2\left(f\right)}{1 - H_2\left(p_\mathrm{b}\right)} \tag{8}$$

with the binary entropy function

$$H_2\left(x\right) = x \log_2\left(\frac{1}{x}\right) + \left(1 - x\right) \log_2\left(\frac{1}{1 - x}\right). \tag{9}$$

The achievable net data rate therefore computes to 6.34 bit/s, assuming $p_\mathrm{b} = 0.01$.

To get an impression of the transmission resilience under changed conditions, a second transmission with a channel length of 10 cm (where we can expect an amplitude attenuation of about 2 dB and an increase of FWHM by 50 % according to the results in Section VI-A) was performed. The achievable net data rate for the doubled transmission distance is 5.19 bit/s.

IX. Conclusion

All testbed components were improved regarding performance in a data transmission scenario and size in comparison to the original setup. The micropump as transmitter is an order of magnitude smaller than the previously used pump and has a higher peak flow rate. More reproducible dispensing behaviour was achieved with a one-way check valve. Three new receivers, with iterative improvements on sensitivity and sample rate, were presented. The SNR of the capacitive sensor setup is more than 30 dB higher than the value for the commercial reference product. Furthermore, a significantly higher sample rate allows for smaller symbol intervals, a scalable sensor design with printed capacitive planes enables flexible adaptation to a given environment. Two-dimensional localisation of MNPs was achieved using multiple planar coils.

As can be seen in Fig. 10, both the transmission efficiency and achievable net data rate was significantly improved throughout the various component refinements. The presented overall data rate of 6.34 bit/s is much higher than shown in the original setup or any other comparable biocompatible testbed (max. 1.6 bit/s in [7]) for molecular communication.

Data transmission is severely influenced by channel length. As shown, an increased channel length causes stronger burst deterioration and requires either an increased injection volume or a reduced data rate. The system therefore has to be specifically adapted or trained for a given transmission channel. Nonetheless, for the example of a doubled distance, data transmission with an overall data rate of 5.19 bit/s was still possible. Scenarios with a significantly changing channel require a sophisticated adaptive communication protocol. Data transmission in very long channels would benefit from a relay system.

Data demodulation using a CNN classifier in a medical application with a high demand on miniaturisation may be challenging. However, the field of edge artificial intelligence is developing rapidly. Further investigation of size and power efficient demodulation approaches using such technology as well as demodulation under changing channel conditions is necessary.

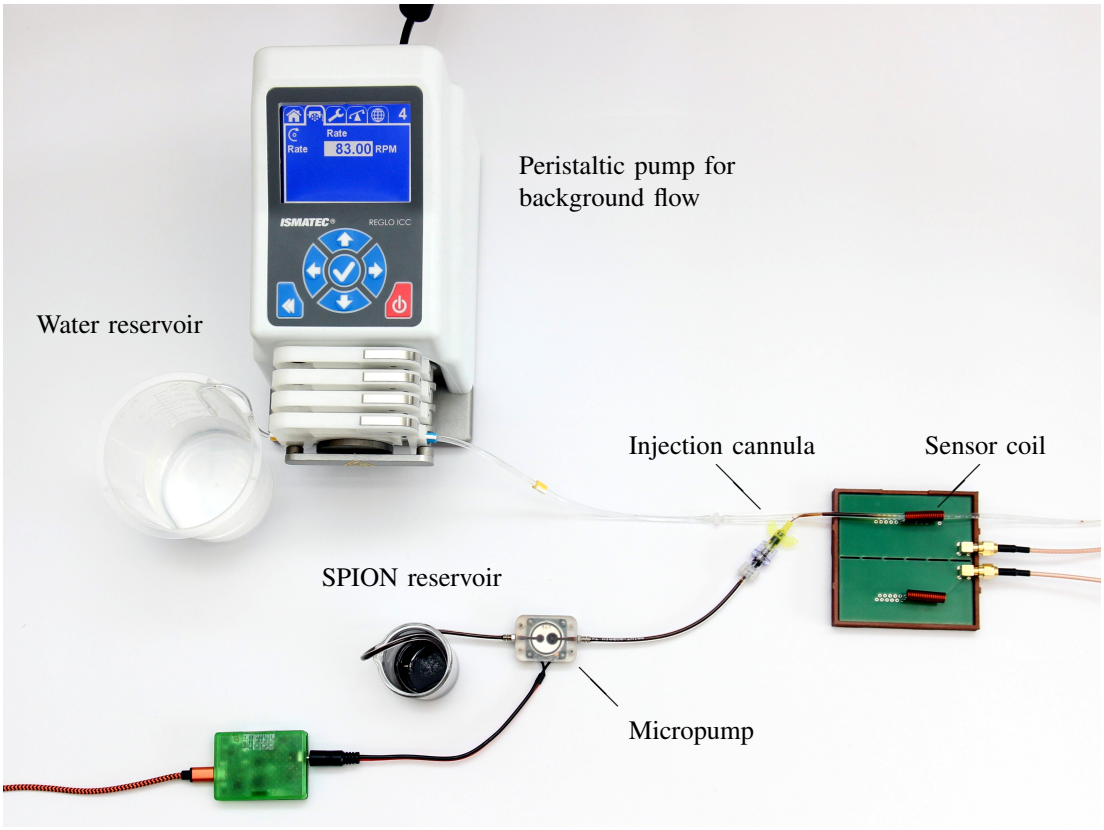

Fig. 9: Complete testbed setup with improved components. The background flow of water is driven by a peristaltic pump. Data is modulated by injecting SPIONs into the background flow with a micropump. The distance from the transmitter to the receiver is 5 cm. The achieved data rate and efficiency is denoted as mark 8 in Fig. 10.

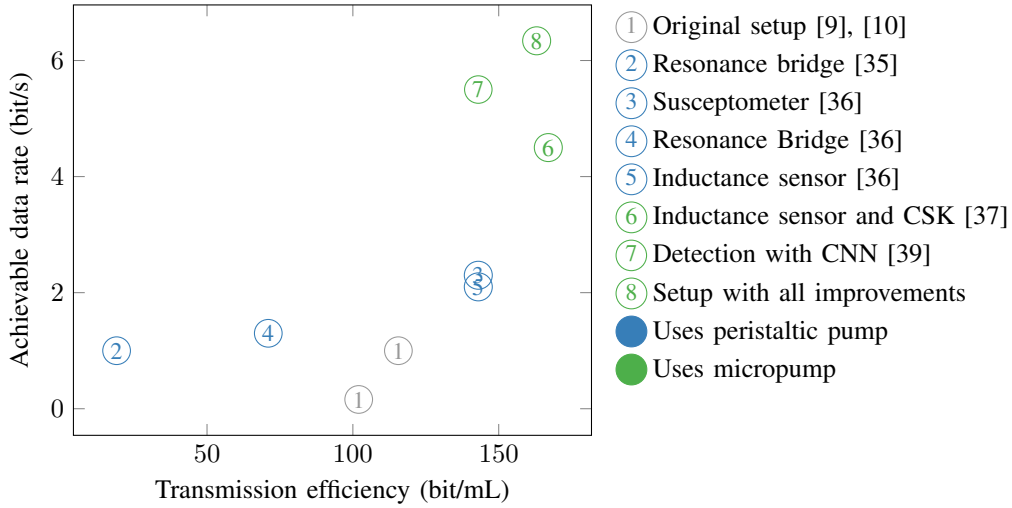

Fig. 10: Overview of possible data rates and average transmission efficiencies shown throughout the evolution of the testbed components. The achievable data rate is calculated according to Shannon's limit, assuming a tolerable remaining bit error rate of $p_\mathrm{b} = 0.01$. The data rate was successfully increased to 6.24 bit/s in comparison to 0.16 bit/s in the original setup. The average transmission efficiency was increased to more than 160 bit/mL.

Similarly, the localised detection method demonstrated in this work may be used for location-based modulation, but requires further research in regard to possible modulation schemes, the impact of crosstalk and other noise sources, and the achievable gain in comparison to CSK.

In the future this testbed will be used for channel model validation and presents a starting point for developing real-life applications of molecular communication in biological systems. We encourage the use of the presented testbed concept for further research.

ACKNOWLEDGMENT

This work was supported in part by the German Federal Ministry of Education and Research (BMBF), project MAMOKO (16KIS0913K).

REFERENCES

[1] N. Farsad, H. B. Yilmaz, A. Eckford, C.-B. Chae, and W. Guo, "A comprehensive survey of recent advancements in molecular communication," *IEEE Communications Surveys & Tutorials*, vol. 18, no. 3, pp. 1887–1919, 2016.

[2] S. Kriegman, D. Blackiston, M. Levin, and J. Bongard, "A scalable pipeline for designing reconfigurable organisms," *Proceedings of the National Academy of Sciences*, vol. 117, no. 4, pp. 1853–1859, 2020.

[3] N. Farsad, W. Guo, and A. W. Eckford, "Tabletop molecular communication: Text messages through chemical signals," *PLOS ONE*, vol. 8, no. 12, pp. 1–13, Dec. 2013.

[4] V. Jamali, A. Ahmadzadeh, W. Wicke, A. Noel, and R. Schober, "Channel modeling for diffusive molecular communication—a tutorial review," *Proceedings of the IEEE*, vol. 107, no. 7, pp. 1256–1301, Jul. 2019.

[5] M. Kuscu, E. Dinc, B. A. Bilgin, H. Ramezani, and O. B. Akan, "Transmitter and receiver architectures for molecular communications: A survey on physical design with modulation, coding, and detection techniques," *Proceedings of the IEEE*, vol. 107, no. 7, pp. 1302–1341, 2019.

[6] A. Al-Helali, B. Liang, and N. Nasser, "Novel molecular signaling method and system for molecular communication in human body," *IEEE Access*, vol. 8, pp. 119 361–119 375, 2020.

[7] B.-H. Koo, H. J. Kim, J.-Y. Kwon, and C.-B. Chae, "Deep learning-based human implantable nano molecular communications," in *ICC 2020 - 2020 IEEE International Conference on Communications (ICC)*, 2020, pp. 1–7.

[8] T. Luo, R. Zheng, J. Song, L. Lin, and H. Yan, "A small-scale modulator of electric-to-biological signal conversion for synthetic molecular communications," in *ICC 2020 - 2020 IEEE International Conference on Communications (ICC)*, 2020, pp. 1–7.

[9] H. Unterweger, J. Kirchner, W. Wicke, A. Ahmadzadeh, D. Ahmed, V. Jamali, C. Alexiou, G. Fischer, and R. Schober, "Experimental molecular communication testbed based on magnetic nanoparticles in duct flow," in *2018 IEEE 19th International Workshop on Signal Processing Advances in Wireless Communications (SPAWC)*, Jun. 2018, pp. 1–5.

[10] W. Wicke, H. Unterweger, J. Kirchner, L. Brand, A. Ahmadzadeh, D. Ahmed, V. Jamali, C. Alexiou, G. Fischer, and R. Schober, "Experimental system for molecular communication in pipe flow with magnetic nanoparticles," *IEEE Transactions on Molecular, Biological and Multi-Scale Communications*, pp. 1–1, 2021.

[11] N. Farsad, D. Pan, and A. Goldsmith, "A novel experimental platform for in-vessel multi-chemical molecular communications," in *GLOBECOM 2017 - 2017 IEEE Global Communications Conference*. IEEE, Dec. 2017.

[12] L. Grebenstein, J. Kirchner, R. S. Peixoto, W. Zimmermann, F. Irnstorfer, W. Wicke, A. Ahmadzadeh, V. Jamali, G. Fischer, R. Weigel, A. Burkovski, and R. Schober, "Biological optical-to-chemical signal conversion interface: A small-scale modulator for molecular communications," *IEEE Transactions on NanoBioscience*, vol. 18, no. 1, pp. 31–42, Jan. 2019.

[13] L. Grebenstein, J. Kirchner, W. Wicke, A. Ahmadzadeh, V. Jamali, G. Fischer, R. Weigel, A. Burkovski, and R. Schober, "A molecular communication testbed based on proton pumping bacteria: Methods and data," *IEEE Transactions on Molecular, Biological and Multi-Scale Communications*, vol. 5, no. 1, pp. 56–62, 2019.

[14] L. Khaloopour, S. V. Rouzegar, A. Azizi, A. Hosseinian, M. Farahnak-Ghazani, N. Bagheri, M. Mirmohseni, H. Arjmandi, R. Mosayebi, and M. Nasiri-Kenari, "An experimental platform for macro-scale fluidic medium molecular communication," *IEEE Transactions on Molecular, Biological and Multi-Scale Communications*, vol. 5, no. 3, pp. 163–175, 2019.

[15] J. Wang, D. Hu, C. Shetty, and H. Hassanieh, *Understanding and Embracing the Complexities of the Molecular Communication Channel in Liquids*. New York, NY, USA: Association for Computing Machinery, 2020.

[16] P. Lu, Z. Wu, and B. Liu, "A vertical channel model of molecular communication and its test-bed," *EAI Endorsed Transactions on Pervasive Health and Technology*, vol. 3, no. 9, 3 2017.

[17] M. Damrath, S. Bhattacharje, and P. A. Hoeher, "Investigation of multiple fluorescent dyes in macroscopic air-based molecular communication," Jan 2021, unpublished.

[18] N.-R. Kim, N. Farsad, C.-B. Chae, and A. W. Eckford, "A realistic channel model for molecular communication with imperfect receivers," in *2014 IEEE International Conference on Communications (ICC)*, 2014, pp. 3987–3992.

[19] N.-R. Kim, N. Farsad, C. Lee, A. W. Eckford, and C.-B. Chae, "An experimentally validated channel model for molecular communication systems," *IEEE Access*, vol. 7, pp. 81 849–81 858, 2019.

[20] P. N. Prasanth, K. P. Sumanth, V. K. Chakka, and G. Roy, "Experimental implementation of molecular communication system using sampling based adaptive threshold variation demodulation algorithm," in *2018 IEEE International Conference on Advanced Networks and Telecommunications Systems (ANTS)*, 2018, pp. 1–5.

[21] A. O. Kislal, B. C. Akdeniz, C. Lee, A. E. Pusane, T. Tugcu, and C.-B. Chae, "Isi-mitigating channel codes for molecular communication via diffusion," *IEEE Access*, vol. 8, pp. 24 588–24 599, 2020.

[22] F. Gulec and B. Atakan, "A droplet-based signal reconstruction approach to channel modeling in molecular communication," *IEEE Transactions on Molecular, Biological and Multi-Scale Communications*, vol. 7, no. 1, pp. 64–68, 2021.

[23] B.-H. Koo, C. Lee, H. B. Yilmaz, N. Farsad, A. Eckford, and C.-B. Chae, "Molecular MIMO: From theory to prototype," *IEEE Journal on Selected Areas in Communications*, vol. 34, no. 3, pp. 600–614, Mar. 2016.

[24] D. T. McGuiness, S. Giannoukos, S. Taylor, and A. Marshall, "Experimental and analytical analysis of macro-scale molecular communications within closed boundaries," *IEEE Transactions on Molecular, Biological and Multi-Scale Communications*, vol. 5, no. 1, pp. 44–55, 2019.

[25] S. Giannoukos, A. Marshall, S. Taylor, and J. Smith, "Molecular communication over gas stream channels using portable mass spectrometry," *Journal of the American Society for Mass Spectrometry*, vol. 28, pp. 2371–2383, 2017.

[26] P. A. Hoeher, M. Damrath, S. Bhattacharjee, and M. Schurwanz, "On mutual information analysis of infectious disease transmission via particle propagation," *IEEE Transactions on Molecular, Biological and Multi-Scale Communications*, p. 1, 2021.

[27] B. Krishnaswamy, C. M. Austin, J. P. Bardill, D. Russakow, G. L. Holst, B. K. Hammer, C. R. Forest, and R. Sivakumar, "Time-elapse communication: Bacterial communication on a microfluidic chip," *IEEE Transactions on Communications*, vol. 61, no. 12, pp. 5139–5151, Dec. 2013.

[28] M. Bartunik, M. Fleischer, W. Haselmayr, and J. Kirchner, "Colour-specific microfluidic droplet detection for molecular communication," in *Proceedings of the 7th ACM International Conference on Nanoscale Computing and Communication*, ser. NanoCom '20. New York, NY, USA: Association for Computing Machinery, 2020.

[29] M. Bartunik, M. Fleischer, W. Haselmayr, and J. Kirchner, "Advanced characterisation of a sensor system for droplet-based microfluidics," in *2020 IEEE SENSORS*, 2020, pp. 1–4.

[30] M. G. Durmaz, A. Dilmac, B. Camli, E. Gencturk, Z. C. Canbek Ozdil, A. E. Pusane, A. D. Yalcinkaya, K. Ulgen, and T. Tugcu, "Preliminary studies on flow assisted propagation of fluorescent microbeads in microfluidic channels for molecular communication systems," in *Bio-inspired Information and Communication Technologies*, Y. Chen, T. Nakano, L. Lin, M. U. Mahfuz, and W. Guo, Eds. Cham: Springer International Publishing, 2020, pp. 294–302.

[31] C. Janko, J. Zaloga, M. Pöttler, S. Dürr, D. Eberbeck, R. Tietze, S. Lyer, and C. Alexiou, "Strategies to optimize the biocompatibility of iron oxide nanoparticles – "spions safe by design"," *Journal of Magnetism and Magnetic Materials*, vol. 431, pp. 281–284, 2017.

[32] T. Neuberger, B. Schöpf, H. Hofmann, M. Hofmann, and B. von Rechenberg, "Superparamagnetic nanoparticles for biomedical applications:

Possibilities and limitations of a new drug delivery system," *Journal of Magnetism and Magnetic Materials*, vol. 293, no. 1, pp. 483–496, 2005, proceedings of the Fifth International Conference on Scientific and Clinical Apllications of Magnetic Carriers.

[33] R. Tietze, S. Lyer, S. Dürr, T. Struffert, T. Engelhorn, M. Schwarz, E. Eckert, T. Göen, S. Vasylyev, W. Peukert, F. Wiekhorst, L. Trahms, A. Dörfler, and C. Alexiou, "Efficient drug-delivery using magnetic nanoparticles–biodistribution and therapeutic effects in tumour bearing rabbits," *Nanomedicine : nanotechnology, biology, and medicine*, vol. 9, no. 7, pp. 961–971, 2013.

[34] T. L. Hennig, H. Unterweger, S. Lyer, C. Alexiou, and I. Cicha, "Magnetic accumulation of spions under arterial flow conditions: Effect of serum and red blood cells," *Molecules (Basel, Switzerland)*, vol. 24, no. 14, 2019.

[35] M. Bartunik, M. Lübke, H. Unterweger, C. Alexiou, S. Meyer, D. Ahmed, G. Fischer, W. Wicke, V. Jamali, R. Schober, and J. Kirchner, "Novel receiver for superparamagnetic iron oxide nanoparticles in a molecular communication setting," in *Proceedings of the Sixth Annual ACM International Conference on Nanoscale Computing and Communication - NANOCOM '19*. ACM Press, Sep. 2019.

[36] M. Bartunik, H. Unterweger, C. Alexiou, R. Schober, M. Lübke, G. Fischer, and J. Kirchner, "Comparative evaluation of a new sensor for superparamagnetic iron oxide nanoparticles in a molecular communication setting," in *Bio-inspired Information and Communication Technologies*. Cham: Springer International Publishing, 2020, pp. 303–316.

[37] M. Bartunik, T. Thalhofer, C. Wald, M. Richter, G. Fischer, and J. Kirchner, "Amplitude modulation in a molecular communication testbed with superparamagnetic iron oxide nanoparticles and a micropump," in *Body Area Networks. Smart IoT and Big Data for Intelligent Health*, M. M. Alam, M. Hämäläinen, L. Mucchi, I. K. Niazi, and Y. Le Moullec, Eds. Cham: Springer International Publishing, 2020, pp. 92–105.

[38] F. M. White, *Fluid mechanics*, 8th ed. New York: McGraw-Hill Education, 2017.

[39] M. Bartunik, J. Kirchner, and J. Reichstein, "Capacitive Sensing for Magnetic Nanoparticles in Molecular Communication," in *The International Instrumentation and Measurement Technology Conference*, 2022, to appear.

[40] R. S. M. Rikken, R. J. M. Nolte, J. C. Maan, J. C. M. van Hest, D. A. Wilson, and P. C. M. Christianen, "Manipulation of micro- and nanostructure motion with magnetic fields," *Soft Matter*, vol. 10, pp. 1295–1308, 2014.

[41] M. Bartunik, O. Keszocze, B. Schiller, and J. Kirchner, "Using deep learning to demodulate transmissions in molecular communication," in *2022 IEEE 16th International Symposium on Medical Information and Communication Technology (ISMICT)*, 2022, pp. 1–6.

Max Bartunik completed his master's degree for electrical engineering in 2019 at the Friedrich-Alexander-Universität Erlangen-Nürnberg (FAU). He is currently pursuing his Ph.D. as a research assistant at the Institute for Electronics Engineering of the FAU. His main research topics are molecular communication and medical electronics.

Georg Fischer (Senior Member, IEEE) received the Diploma degree in electrical engineering with a focus on communications and microwave from RWTH Aachen University, Aachen, Germany, in 1992, and the Dr. Ing. degree in electrical engineering from the University of Paderborn, Germany, in 1997. From 1993 to 1996, he was a Research Assistant with the University of Paderborn, where he was involved in adaptive antenna array systems for mobile satellite communications. From 1996 to 2008, he performed research with Bell Laboratories, Lucent (later Alcatel-Lucent), where he focused on the RF and digital architecture of mobile communication base stations for global system for mobile communications (GSM), universal mobile telecommunications system, and features for network coverage and capacity enhancements. In 2000, he became a Bell Laboratories Distinguished Member of Technical Staff, and in 2001, he became a Bell Laboratories Consulting Member of Technical Staff. He also acted as the Chairman of the European Telecommunications Standards Institute during the physical-layer standardization of the GSM-EDGE system. From 2001 to 2007, he was a part-time Lecturer with the University of Erlangen-Nuremberg, Germany. During that time, he lectured on base station technology. Since 2008, he is a Professor of Electronics Engineering with the University of Erlangen–Nuremberg. He holds over 50 patents concerning microwave and communications technology. His current research interests concentrate on medical electronics, such as using microwaves for detection of vital parameters. He is also a Senior Member of the IEEE Microwave Theory and Techniques, Antennas and Propagation, Computer Society, and Vehicular Technology Society and a member of VDE-ITG and the European Microwave Association.

Jens Kirchner studied physics at FAU and at University of St. Andrews, Scotland. He received his doctorates in 2008 and 2016 from FAU in the fields of biosignal analysis and philosophy of science to the Dr. rer. nat. and Dr. phil, respectively. Between 2008 and 2015 he worked at Biotronik SE & Co. KG in Erlangen and Berlin in the research and development of implantable cardiac sensors. Since 2015, he is with the Institute for Electronics Engineering at FAU, where he heads the Medical Electronics & Multiphysics Systems group. His research interests lie in wearable and implantable sensors, inductive power transfer, and molecular communication. He is a Senior Member of the IEEE with membership in the Communications Society, the Magnetics Society and the Engineering in Medicine and Biology Society.